Subsonic and Supersonic Combustion Using Noncircular Injectors

E. Gutmark,* K. C. Schadow,† and K. J. Wilson‡
Naval Weapons Center, China Lake, California 93555

Nonreacting and combustion tests were performed for subsonic, sonic, and supersonic conditions using noncircular injectors in a gas generator combustor. The noncircular injectors, including square, equilateral-, and isosceles-triangular nozzles, were compared to a circular injector. The flowfields of the jets were mapped with hot-wire anemometry and visualized using spark schlieren photography. The combustion characteristics were visualized by high-speed photography and thermal imaging, and the temperature distribution was measured by a rake of thermocouples. The present tests conducted at high Reynolds and Mach numbers confirmed earlier results obtained for the low range of these numbers, i.e., the combination of large-scale mixing at the flat sides with the fine-scale mixing at the vertices is beneficial for combustion. Large-scale structures provide bulk mixing between the fuel and air, whereas fine-scale mixing contributes to the reaction rate and to better flameholding characteristics.

Nomenclature

A = side length of square and equilateral triangle jet and base length of isosceles
D = diameter
H = height of triangle
M = Mach number
m = mass flow rate
P = pressure
Re = Reynolds number
r = radial coordinate
T = temperature
U = mean velocity
u' = turbulent velocity
x = axial coordinate
ν = kinematic viscosity
ϕ = equivalence ratio

Subscripts

A = air
CH = ethylene
CL = centerline
c = combustion
e = equivalent (having the same area as the circular jet)
GG = gas generator
O = oxygen
SL = shear layer
t = throat
0 = exit condition
0.5 = half-width of jet

Introduction

EARLIER studies[1-4] of jets emerging from noncircular nozzles with corners, e.g., triangular, rectangular, or square nozzles, showed that the introduction of sharp corners in the outlet nozzle can significantly increase the small-scale turbulence intensity at the corners relative to the flat segments of the nozzle. It was also shown that while highly coherent structures can be generated at the flat sides, only small-scale turbulent flow emanated from the corners.[5-7] This small-scale turbulence was generated by axial vortices formed in the corners inside the nozzle[8] and augmented by strong vortex bending induced by the highly curved flow at the corners.[9-10] The vortex bending and self-induction process also increased the spreading rate of the jet at the flat sides.

The jet orifice geometries that were studied included an isosceles triangle with an apex of 30 deg, an equilateral triangle, and a square (90-deg vertex). The thickness of the boundary layer at the corner is larger than at the flat side. The momentum thickness ratio between the two is changing with the corner's angle: 2.9 for the 30-deg corner and 1.5 for the 90-deg corner. The thicker shear layers have a lower spreading rate. Farther downstream, as the flat-side shear layers grow thicker, the corner sections become more active, amplifying the local instability modes that have larger phase velocity, leading to local vortex bending and further increase of the flat-side spreading rate.[10] The peripheral variation of the mean and turbulent flowfield resulted in large azimuthal variations of the jet growth pattern. The strong amplification of the turbulent fluctuations at the flat sides resulted in an increase in the jet spreading rate due to nonlinear interaction of the turbulence with the mean flow.[11] The variation of the spreading rate around the jet circumference caused changes in the geometry of its cross section.

These special flow features of nozzles with corners were tested in a reactive flow of square and triangular flames.[12] The flow behavior observed in cold flows affected the results in the reacting tests. Combustion at the flat segments was confined in periodic, large-scale coherent structures, whereas, at the corners, combustion occurred in randomly distributed small-scale flamelets. The difference between the two flame sections was more pronounced for small corner angles.

The coexistence of regions with large-scale structures and others with fine-scale structures in the same flow of triangular and square jets is advantageous for combustion systems. The enhanced fine-scale mixing at the corners makes this section the best location to initiate combustion. The highly turbulent flow at the corners helps to start the reaction close to the nozzle exit, which increases the local temperature of the combustion products since a reduced amount of cool air is entrained into the reaction region. At the flat sections of the shear flow, the large-scale mixing provides the necessary amounts of air to sustain combustion. This combination of large- and fine-scale structures was shown to be advantageous to reduce combustion instabilities in dump combustors.[13] This instability, which develops from interaction between the large-scale structures in

Received May 23, 1989; revision received Nov. 8, 1989.

*Research Scientist, Research Department. Member AIAA.
†Supervisory General Engineer, Research Department.
‡Aerospace Engineer, Research Department.

the flow and the combustor acoustic modes,[14,15] can be controlled by reducing the coherence of the flow structures using inlets with corners.[7,12]

The basic understanding obtained in low Reynolds number subsonic nonreacting and reacting flows is extended, in the present work, to higher Reynolds number free and ducted subsonic and supersonic flows in nonreacting and combusting conditions. In the reacting tests, nozzles with corners were tested for fuel-rich plume combustion in a subsonic, coaxial airstream.

Experimental Apparatus

The cold flow tests were done in a freejet facility using hot-wire anemometry. Nozzles having square, equilateral-triangular, and isosceles-triangular cross sections were adapted smoothly at the end of a circular pipe to study the shear-flow development for vertex angles of 90, 60, and 30 deg. All of the tested nozzles are shown in Fig. 1. The direction and origin for measuring radial distances are defined in this figure. The dimensions of the nozzles used for the hot-wire measurements and flame visualization are given in Table 1. The jets were operated at sonic and supersonic exit velocities, with a Reynolds number, based on the equivalent diameter D_e and the exit velocity U_0 of up to $Re = U_0 D_e/\nu = 650{,}000$. The equivalent diameter for the noncircular jet was defined as the diameter of a circle having the same exit area as the noncircular jet exit area.

A hot-wire system with a 50-kHz frequency response was used for the flowfield measurements. The hot-wire holder was mounted on a computer-controlled three-axis traverse mechanism. A VAX 750 microcomputer was used for calibration, data acquisition, and subsequent data analysis.

In the combustion experiments, nozzles with corners were used at the outlet of a fuel-rich gas generator. The effect of the corners on the fuel-rich plume combustion were studied using high-speed photography, thermal imaging, and thermocouples. A gas generator burning ethylene, oxygen, and nitrogen was used to simulate fuel-rich solid propellant reaction products (see Fig. 2). The gaseous fuels were ignited in the gas generator by a hydrogen/oxygen-pilot igniter (not shown). Mass flow rate of air was $\dot{m}_A = 1$ kg/s, and the fuel-air mixture in the gas generator was $0.040 < \dot{m}_{CH} < 0.051$ kg/s, $\dot{m}_0 = 0.038$ kg/s, and $\dot{m}_A = 0.050$ kg/s. The gas generator operated in an equivalence ratio range of $2.5 < \phi < 3.2$ and temperatures between 1550 to 1800 K.

Table 1 Dimensions of nozzles (in mm)

	Nozzle								
	Square		Equilateral triangle			Isosceles triangle			Circle
Tests	A	D_e	A	H	D_e	A	H	D_e	D
Cold flow	17	19.2	25	22	18.7	18	33.5	19.6	19
Flame	17	19.2	22	19	16.3	18	33.5	19.6	19

The radiance intensity of the plume was measured using a thermal imaging camera, AGA Model 750 Thermovision. This camera has a single detector element which scans the object in a raster pattern containing 74 active lines at a rate of 25 fields/s. Each line contains 100 resolution elements. All optical elements are wideband coated. The camera, equipped with a narrow-band filter, was operated at a spectral band of 4.1–4.9 μ.

The signal from the infrared camera was acquired at 25 frames/s using a custom-constructed time corrector with a transient digitizer interfaced to a personal computer. The digitizer allows acquisition of up to 256 frames at once, which are transferred to the personal computer for immediate contour display, analysis, and archiving.

The camera was calibrated for spectral response, responsivity, and field of view. The spectral response is measured using a monochromator. The camera and the thermocouple of the monochromator share a narrow spectral band output

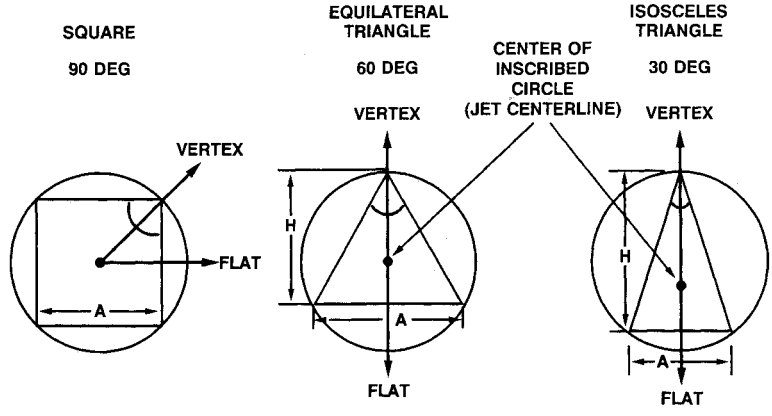

Fig. 1 Configuration of the noncircular nozzles.

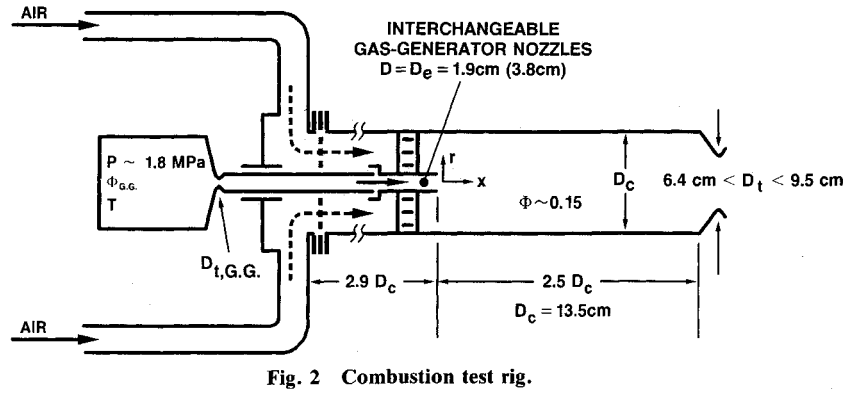

Fig. 2 Combustion test rig.

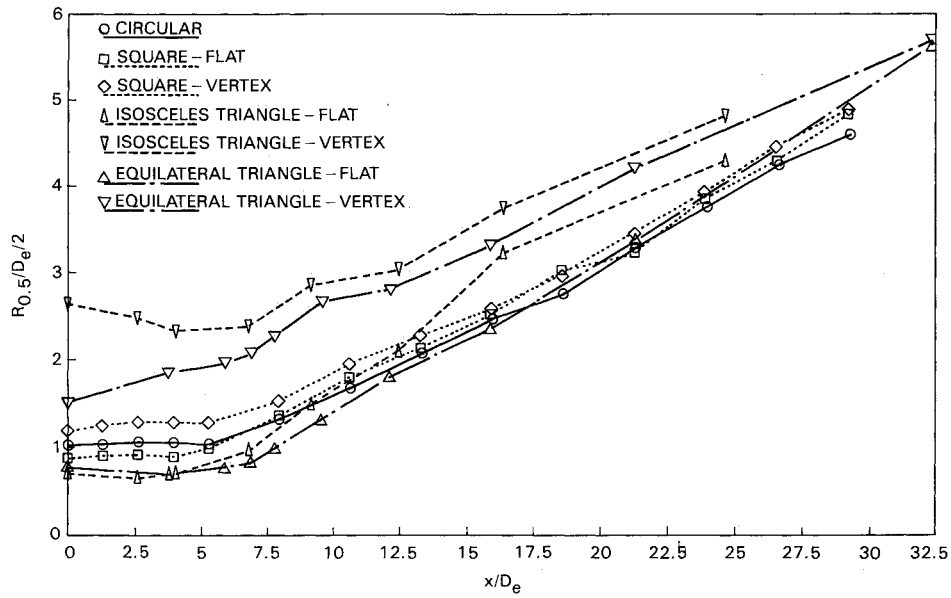

Fig. 3 Comparison of the variation of the jet half-width for the circular, square, equilateral-, and isosceles-triangular jets with sonic exit velocity.

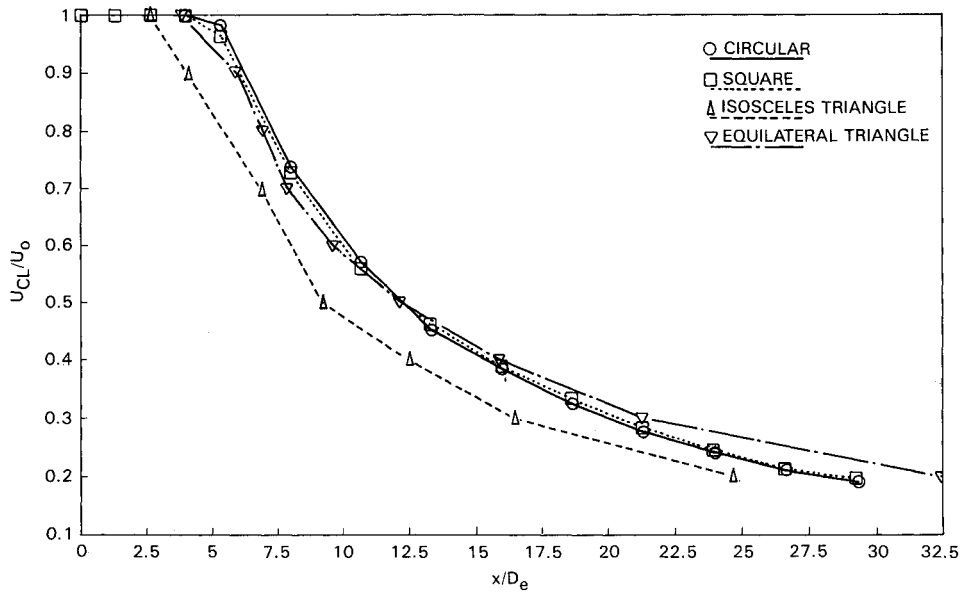

Fig. 4 Mean velocity decay along the centerline of the jet for the circular, square, equilateral-, and isosceles-triangular jets with sonic exit velocity.

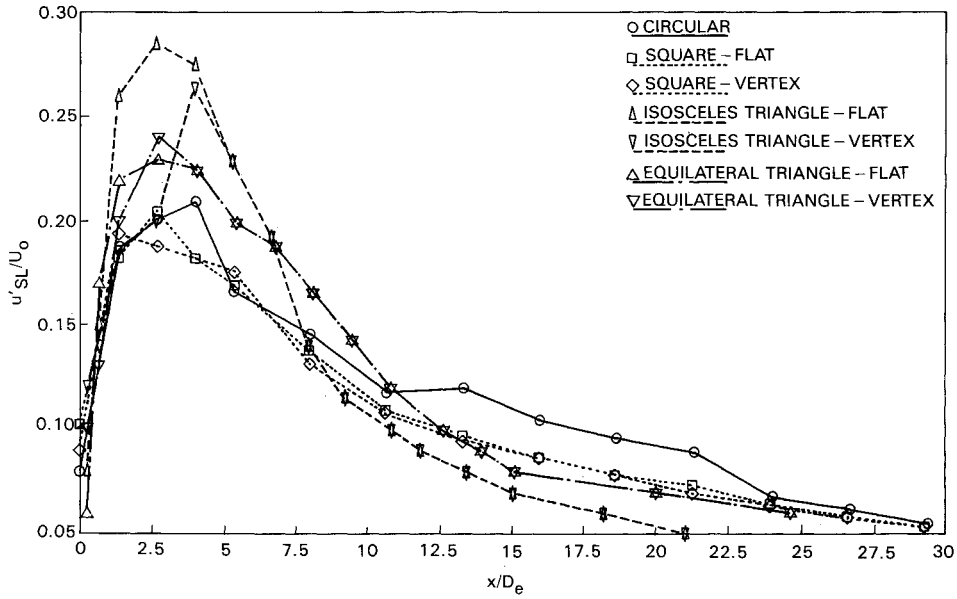

Fig. 5 Maximum turbulence intensity variation along the shear-layer center for the circular, square, equilateral-, and isosceles-triangular jets with sonic exit velocity.

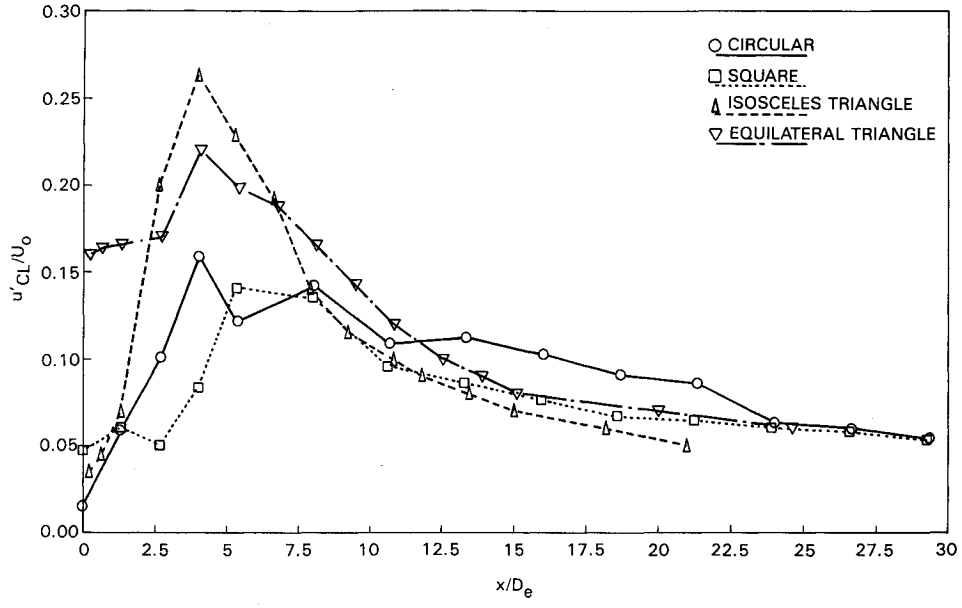

Fig. 6 Turbulence intensity variation along the jet centerline for the circular, square, equilateral-, and isosceles-triangular jets with sonic exit velocity.

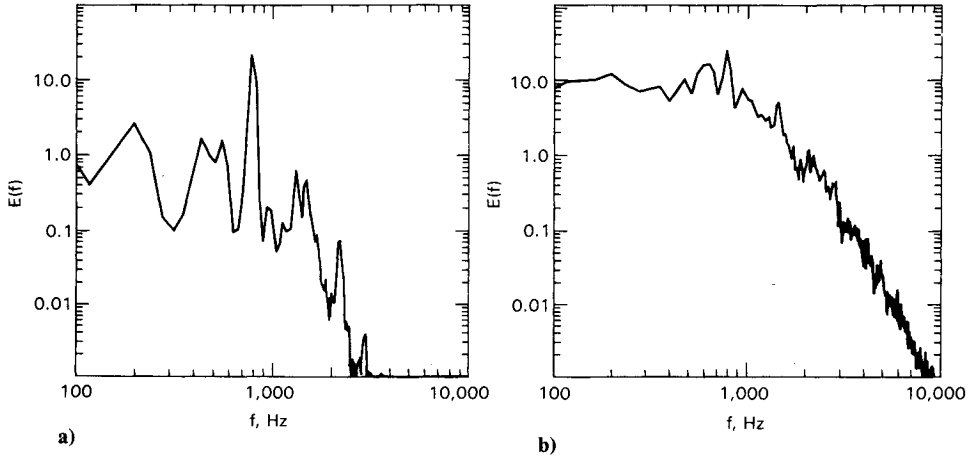

Fig. 7 Normalized power spectra of the turbulent velocity fluctuations for the flat side: a) vertex; b) measured at $x/D_e = 0.2$ for sonic exit velocity.

beam (<0.03 μ), and the signals are ratioed over the wavelength region being used. The optical paths from the source to the thermocouple and camera are purged with dry nitrogen to reduce atmospheric absorption.

Temperature measurements during the combustion test were obtained using tungsten/rhenium thermocouples in the flowfield near the gas generater nozzle. The thermocouple was compensated, but was not corrected for radiation and combustion losses. The error in temperature measurements is lower than 10%.

Results and Discussion

Nonreacting Tests

Nonreacting tests at sonic and supersonic (underexpanded condition) speeds were conducted using hot-wire anemometry for flowfield measurements and schlieren flow visualization. The equilateral-triangular jet, isosceles triangle with 30-deg apex, and a square jet were compared to a circular jet having the same equivalent exit area and Reynolds number. The same jets were used later for the combustion tests.

The spreading rates of the four jets are compared in Fig. 3, where the jet half-width $R_{0.5}$ is shown as a function of the downstream distance x. The $R_{0.5}$ is defined as the radial distance from the axis (as defined in Fig. 1) to the location where the mean velocity drops to half of the centerline velocity. Some of the features measured for subsonic jets were also observed here. The spreading rate of all of the noncircular jets was larger at the flat sides relative to the vertices sides. The differences between the two sides were most pronounced for the smallest corner angle of the isosceles triangle. The triangle evolved downstream to acquire a circular shape, and no axis switching was observed. The equilateral jet initially had a constant width at the flat side, but for $x/D_e > 6$ the spreading rate increased, and the two sides, which initially have a width ratio of 2:1, are equal at $x/D_e = 32$. The square jet has a zero spread at both the vertex and flat sides for $x/D_e < 5$. For larger axial distance, the spread at the flat side is higher such that the jet becomes axisymmetric at $x/D_e > 17$.

The differences in spreading rates between the four jets also result in a different mean velocity decay along the centerline (see Fig. 4). The circular jet has the longest potential core ($x/D = 6$). The square and the equilateral triangle are similar with slightly larger decay rate. The isosceles triangle has the shortest potential core ($x/D_e = 3$) and its centerline (as defined in Fig. 1) mean velocity is lowest in the present measurement range. The isosceles-triangular jet also has highest initial turbulence intensity at the vertex (see Fig. 5). The amplification of the turbulence fluctuation at this side was low in comparison to the high amplification obtained at the flat sides, which

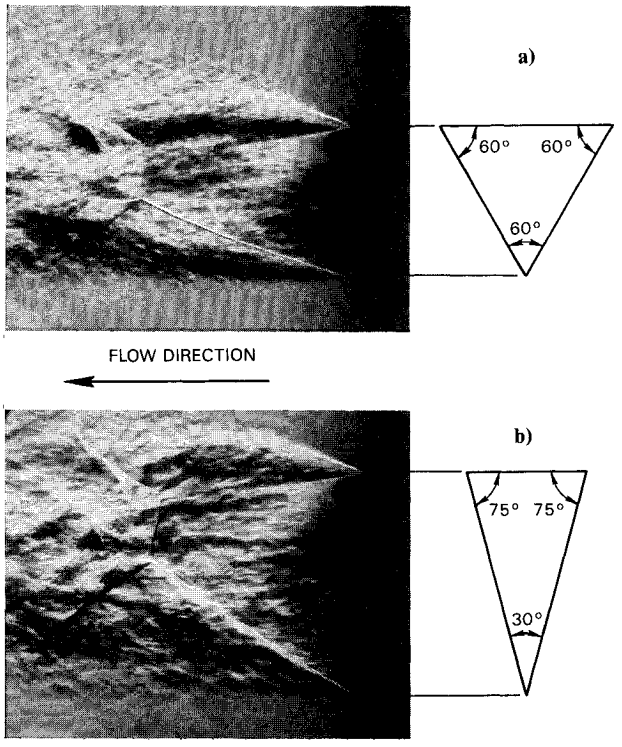

Fig. 8 Schlieren flow visualization: a) the equilateral-triangular jet; b) the isosceles-triangular underexpanded jet (fully expanded Mach number of 2).

reaches a higher level at $x/D_e < 2$. Similar behavior was observed in the equilateral-triangular jet. The square jet had the same amplification at the side and the vertex, and both were similar to the circular jet. As a result of the initial high turbulence level at the vertices and the amplification at the flat sides, the turbulence level at the center of both triangular jets is higher than that of a circular jet (see Fig. 6).

The differences of the turbulence structure between the flat and vertex sections of the equilateral-triangular jet are demonstrated in the spectra shown in Fig. 7. The spectra were measured at $x/D_e = 0.2$, in the center of the shear layers. The power spectrum of the velocity fluctuations measured at the flat side has a sharp peak at the coherent vortex shedding frequency, while the power spectrum measured at the vertex is broadband, signifying a fully developed turbulent flow. The small-scale turbulence content in the vertex section is significantly higher than in the corner flow.

The jets were tested using the convergent-only nozzle at underexpanded conditions, with a nozzle pressure ratio of 7.8 to yield a fully expanded jet Mach number of 2 downstream of the nozzle. At this higher Mach number, the difference between the vertices and flat sides is further accentuated (see the equilateral triangle in Fig. 8a and the isosceles triangle in Fig. 8b). The interaction between the shock waves of the underexpanded jet and the shear layers at the two sides of the jet results in enhanced turbulence at the vertex and increased spreading at the flat sides. The thicker shear layer emanating from the vertices diffuses the shocks faster than at the flat sides. The stronger shocks and the flat side interact with the thinner shear layer to produce larger acoustical emission, which propagate upstream outside the jet and excite the initial shear layer, resulting in a subsequent larger spreading and enhanced large-scale mixing at these sections.[16]

Combustion Tests

The special features of the noncircular nozzles with corners, which were determined for nonreacting flows, were tested in gas generator combustion tests. The radial temperature distribution was measured at three downstream axial distances for the circular, square, equilateral-, and isosceles-triangular nozzles. The tests were done at subsonic, sonic, and supersonic speeds.

Subsonic Tests, $M = 0.4$

The temperature profiles measured at $x/D = 0.7$, 2, and 4.7 for a circular injector are shown in Fig. 9. The double-inflection initial profile at $x/D = 0.7$ is typical of an unstable flame, which is detaching and reattaching intermittently to the nozzle.[9] The higher center part temperatures are associated with the attached flame and the outer, lower, and wider temperature profile is characteristic of a lifted flame. At $x/D = 2$, the higher turbulence and improved mixing in the shear layer result in an increased temperature in the shear-layer region, with a peak temperature at $r/D = 0.8$. The flame temperature becomes more homogeneous radially further downstream ($x/D = 4.7$), toward the end of the jet's potential core.

The noncircular nozzles had different flame characteristics related to the variation of the flow structure around the nozzle. The combustion of the fuel-rich exhaust gases of the square gas generator injector nozzle is shown in Fig. 10. The enhanced turbulence level at the vertices (see Fig. 6) results in the initiation of the flame at the corners, closer to the nozzle with the flame held at the corners. The flame at the flat sides starts farther downstream. This observation is verified in the temperature profiles presented in Fig. 11, where the profiles measured in the plane intersecting the middle points of the square sides are compared to the profiles measured on the diagonal planes. The $r/D_e = 0$ point is located in the square center. Higher temperatures are obtained at the vertices relative to the sides both at $x/D_e = 0.3$ and 1.7. The intermittent liftoff of the flame at the sides is demonstrated by the

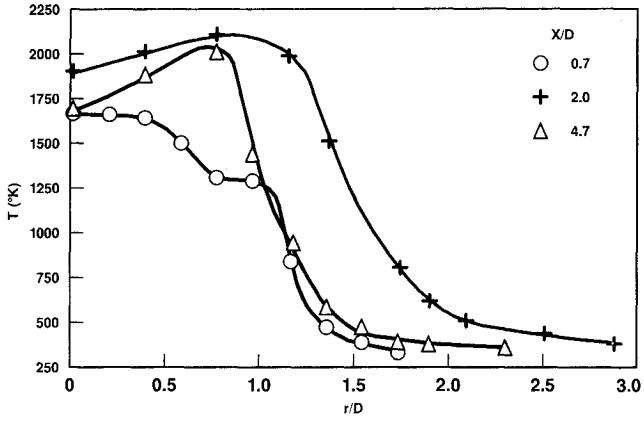

Fig. 9 Temperature profiles of the gas generator with a subsonic circular injector.

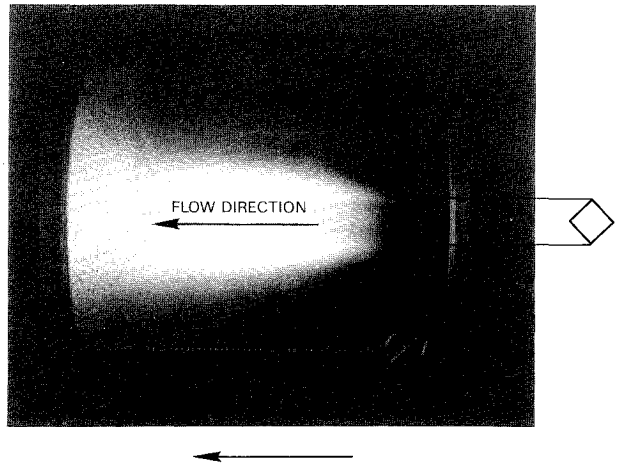

Fig. 10 Photograph of plume combustion downstream of the gas generator exhaust with a square injector.

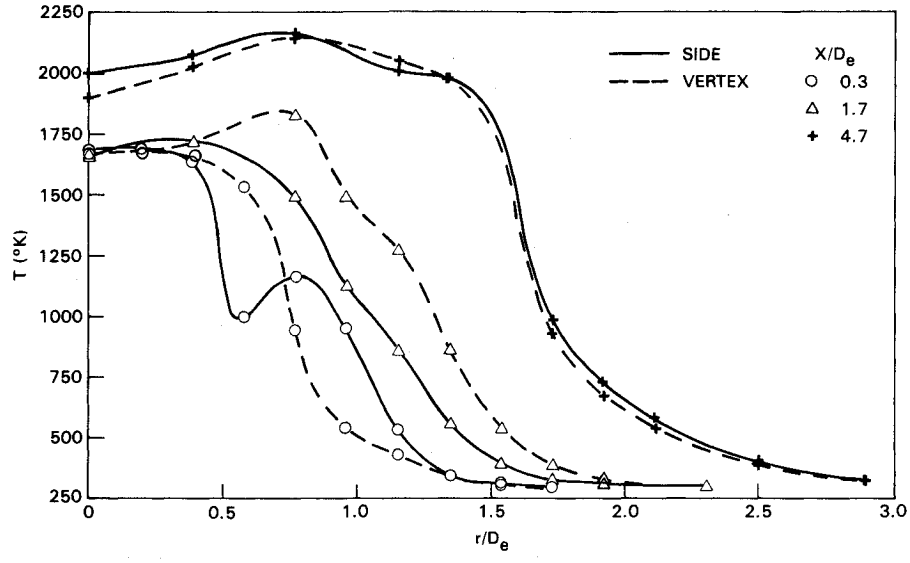

Fig. 11 Temperature profiles of the gas generator combustion using a subsonic square injector.

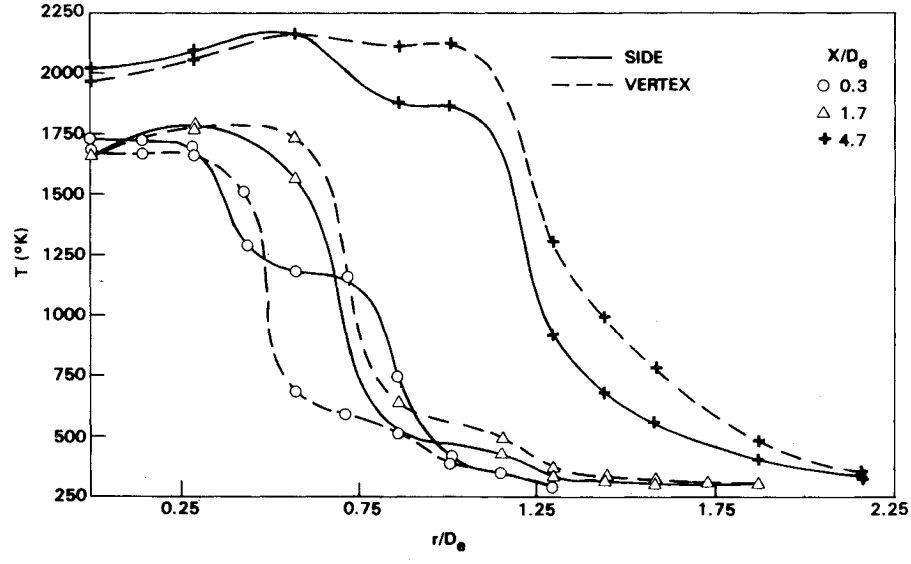

Fig. 12 Temperature profiles of the gas generator combustion using a subsonic equilateral-triangular injector.

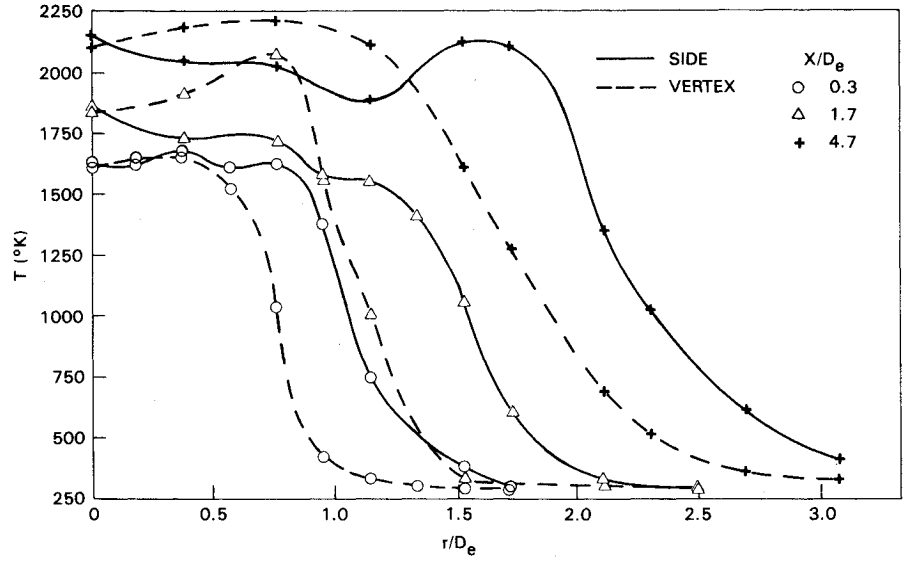

Fig. 13 Temperature profiles of the gas generator combustion using a subsonic isosceles-triangular injector.

double hump profile at $x/D_e = 0.3$. When the flame is attached, its width is significantly smaller than when it is lifted off. The time-averaged measurement combines these two conditions into one profile. At the downstream point of $x/D_e = 4.7$, the flame becomes quasicircular, and the two profiles are congruent.

The differences between the vertex and side sections in the flame become more conspicuous as the corner angle is decreased. This is demonstrated by comparing the temperature profiles of the equilateral-triangular nozzle (vertex angle of 60 deg) given in Fig. 12 and the isosceles-triangular nozzle (vertex angle of 30 deg) in Fig. 13. The $r/D_e = 0$ point is located in the center of the inscribed circle. In both flames, the temperatures at the vertices (indicated by the solid lines) are higher for $x/D_e \geq 1.7$. Also, as shown in the nonreacting flow, the spreading rate is larger at the flat side of the isosceles triangle relative to the vertex, as indicated by the larger extent of high temperatures at the side (see Fig. 13).

The combination of large-scale mixing at the flat sections and small-scale turbulence at the corner[6] is most effective for the isosceles triangle which has the smallest acute apex angle (<60 deg) relative to the other nozzle goemetries described. The initiation of the combustion closer to the nozzle results in higher overall temperature, because the combustion occurs at a location where the amount of entrained air is sufficient to complete the chemical reaction and before the amount of ambient cold air entrained are too high and cause a reduction in the plume temperature. Based on the temperature measurements, the combustion was more intense using the different noncircular nozzles relative to a circular injector. The isosceles triangle gave the highest combustion temperatures, followed by the equilateral triangle. The square was similar to the circular jet.

Sonic Tests

The temperature profiles of the circular, square, and equilateral-triangular nozzles at sonic exit flow are shown in Fig. 14 at $x/D_e = 1.7$ and in Fig. 15 at $x/D_e = 3.7$. The temperature distributions at $x/D_e = 1.7$ were nearly symmetric for the sides and vertices sections of the square and the equilateral triangle. These temperatures were slightly higher than the circular flame for $r/D_e < 0.7$, even though the circular profile was measured farther downstream at $x/D = 2$, where higher temperatures are expected. At $x/D_e = 3.7$ (see Fig. 15), the temperature at the vertices was significantly higher than at the sides, for both the square and triangular nozzles. The cir-

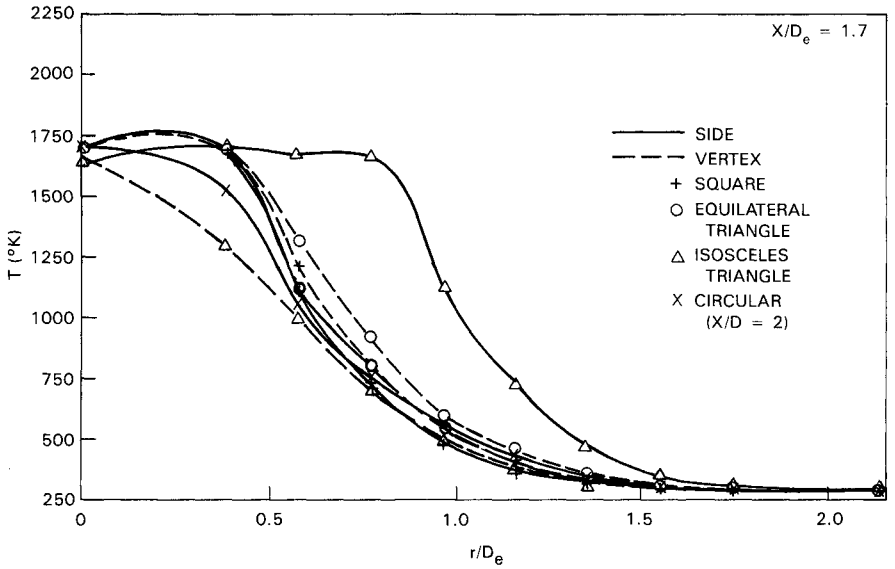

Fig. 14 Temperature profiles of the gas generator combustion using a sonic circular, square, and equilateral-triangular injectors ($x/D_e = 1.7$).

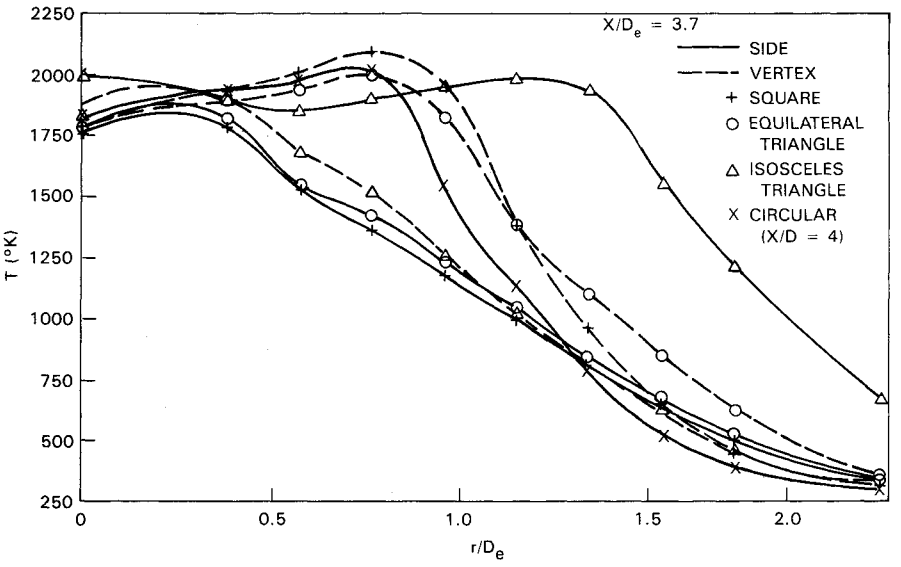

Fig. 15 Temperature profiles of the gas generator combustion using a sonic circular, square, and equilateral-triangular injectors ($x/D_e = 3.7$).

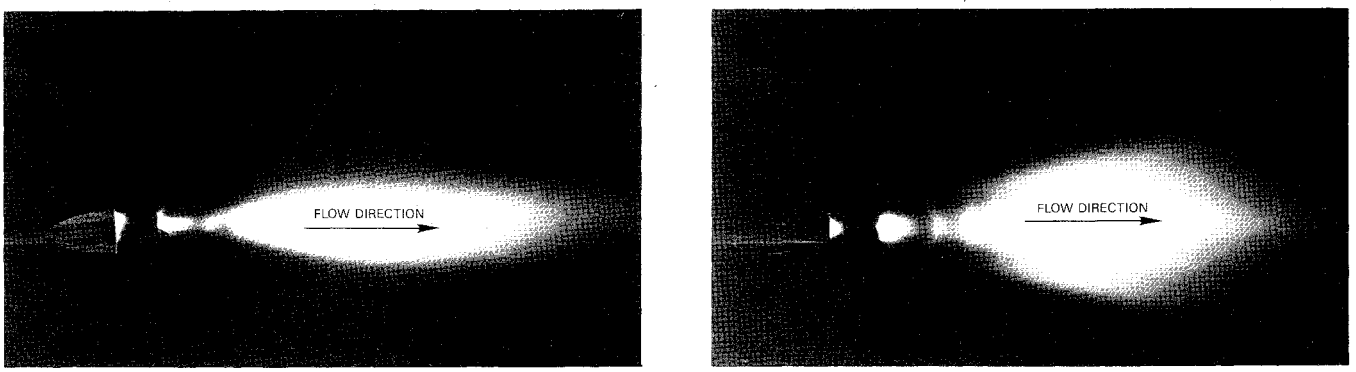

Fig. 16 Photograph of the supersonic isosceles-triangular flame: a) view of the plane including the apex and base center; b) view of the base side.

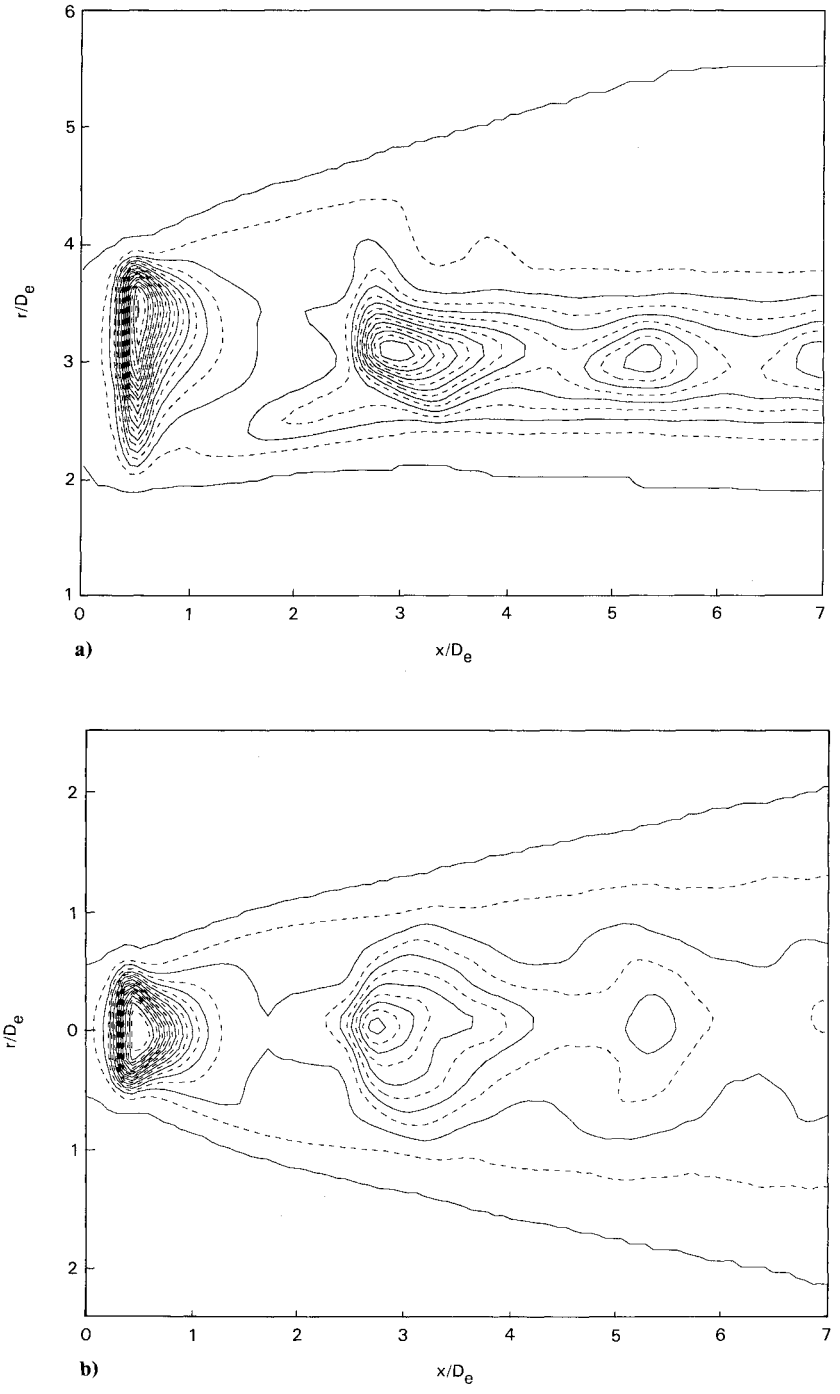

Fig. 17 Thermal image of the supersonic isosceles-triangular flame: a) view of the plane including the apex and base center; b) view of the base side.

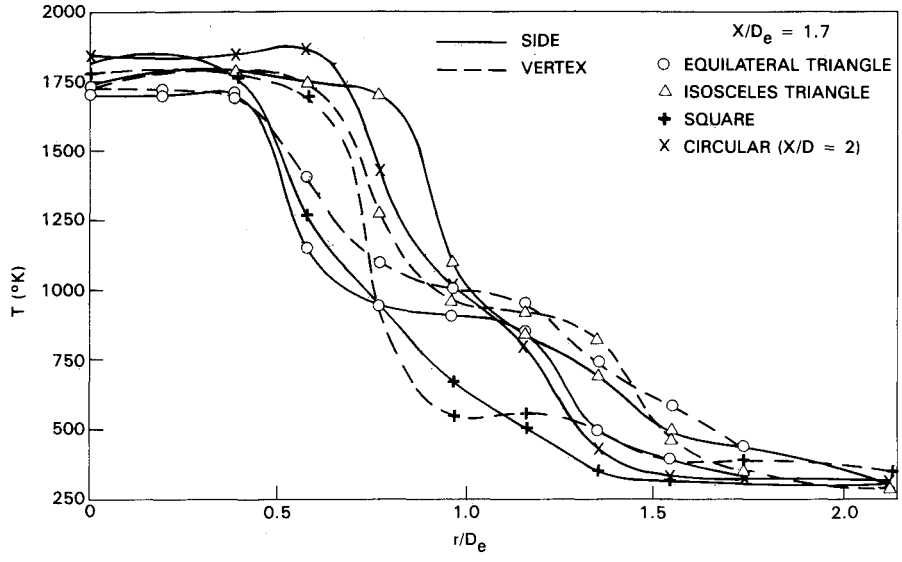

Fig. 18 Temperature profiles of the gas generator combustion using a supersonic circular, square, equilateral-, and isosceles-triangular injectors (x/D_e = 1.7).

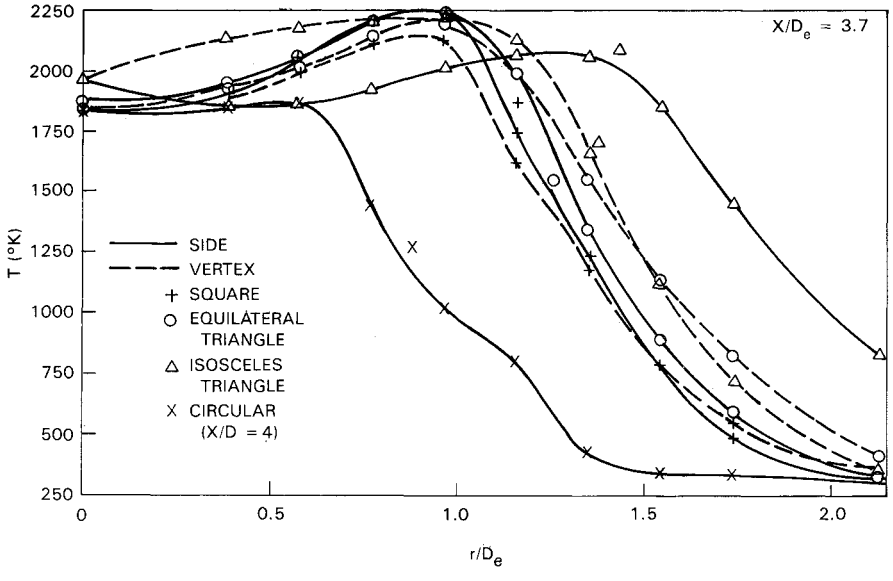

Fig. 19 Temperature profiles of the gas generator combustion using a supersonic circular, square, equilateral-, and isosceles-triangular injectors (x/D_e = 3.7).

cular flame temperature, measured slightly farther downstream, at x/D = 4, was lower at the outer region, for $r/D_e > 1.1$.

Supersonic Tests

The supersonic combustion tests were run at underexpanded flow conditions. In the nonreacting flow section, the flow was dominated by shock cells, which altered the jet behavior at the vertex and flat sides resulting in a large growth at the sides (see Fig. 8). Similar behavior can be observed in the photograph of the reacting isosceles-triangular nozzle shown in Fig. 16a in a plane parallel to the triangle mid-base/vertex plane and Fig. 16b in a view of the base side. The shock cells in the flame were visible up to x/D_e = 9, especially in Fig. 16b. The flame was held at the Mach disk formed downstream of the nozzle, due to the temperature increase at this location. The large spreading at the two long equal sides of the triangle is also clear in Fig. 16b. Similar behavior is demonstrated by the thermal images of the same flame shown in Fig. 17a looking at the plane crossing the apex and the base center and in Fig. 17b from the triangle base. The radiance intensity downstream of the Mach disk is increased, corresponding to the flame shown in Fig. 16. Three shock cells can be observed in the first 5 equivalent diameters downstream of the nozzle. The radiance intensity drops due to the flame expansion. The flame at the vertex side stays at a constant width, and some spread is observed at the base (see Fig. 17a). At the symmetric plane shown in Fig. 17b, the periodic changes in the flame width due to the shock-cell structure are visualized.

The temperature profiles of the three noncircular flames are compared to the circular one in Fig. 18 at x/D_e = 1.7 and in Fig. 19 at x/D_e = 3.7. At the upstream station, the square and equilateral-triangular flames show higher temperatures at the vertex relative to the side, especially in the outer regions of the flame. The isosceles-triangular flame is different, with a higher temperature at the flat side, probably due to the strong asymmetric shock structure. Further downstream, at x/D_e = 3.7, the square and equilateral-triangular flames reach a quasiaxisymmetric structure. The isosceles triangle has a higher temperature at the vertex inner section of the flame; however, the flame spreads faster at the flat side resulting in a higher temperature at $r/D_e > 1$.

Conclusions

1) The structure of the sonic noncircular jets with corners is similar to the subsonic one. The initial vorticity at the corners is smaller than at the sides, yielding a lower amplification of turbulent fluctuations. At the flat sides, the higher amplification results in a larger spreading rate due to energy exchange between the mean and the turbulent flow. Although the amplification is lower at the vertices, the initial turbulence level there is much higher as a result of the corner axial vortices generated in the nozzle.

2) In the supersonic underexpanded jets, the shock structure determines the evolution of the jet. The asymmetry of the expansion waves originating from the flat and vertex sides induces high spread at the flat side and nearly zero spread at the vertex. At high-pressure ratio, a Mach disk is formed in the jet core, and several shock cells can be discerned, generating periodic narrowing and widening of the jet width.

3) Temperature measurements in the combustion tests show increased combustion intensity in the corner sections due to higher turbulence intensity, resulting in higher temperatures at these locations. The temperature at the flat sides is higher at larger radial locations, due to the larger spreading rate of the flame.

4) The effect of the corner on the combustion characteristics increases with decreasing corner's angle. The overall combustion intensity was highest for the isosceles triangle, whereas the square flame was similar to the circular one.

5) For the supersonic flames, the shock structure dominated the combustion. The temperature increase behind the Mach disk and the decrease downstream of an expansion fan periodically change the combustion intensity, resulting in a change of the flameholding location and temperature distribution.

References

[1]Sforza, M. P., Steiger, M. H., and Trentacoste, N., "Studies in Three-Dimensional Viscous Jets," *AIAA Journal*, Vol. 4, No. 5, 1966, pp. 800–806.

[2]Trentacoste, N., and Sforza, M. P., "Further Experimental Results for Three-Dimensional Jets," *AIAA Journal*, Vol. 5, No. 5, 1967, pp. 885–891.

[3]Sfeir, A. A. "Investigation of Three-dimensional Turbulent Rectangular Jets," *AIAA Journal*, Vol. 16, 1978, pp. 1055–1060.

[4]Krothapalli, A., Bagdanoff, D., and Karamcheti, K., "On the Mixing of a Rectangular Jet," *Journal of Fluid Mechanics*, Vol. 107, 1981, pp. 201–220.

[5]Schadow, K. C., Wilson, K. J., and Gutmark, E., "Reduction of Flow Coherence in a Forced, Subsonic Ducted Flow with Dump," AIAA Paper 85-1109, July 1985.

[6]Gutmark, E., Schadow, K. C., Parr, D. M., Harris, C. K., and Wilson, K. J., "The Mean and Turbulent Structure of Noncircular Jets," AIAA Paper 85-0543, March 1985.

[7]Schadow, K. C., Gutmark, E., Parr, T. P., Parr, D. M., and Wilson, K. J., "Selective Control of Flow Coherence in Triangular Jets," *Experiments in Fluids*, Vol. 6, June 1988, pp. 129–135.

[8]Nikuradse, J., "Turbulente Strömung in Nichtreisförmigen Rohren," *Ing. Arch.*, Vol. 1, 1930, pp. 306–332.

[9]Dhanak, M. R., and Debernardinis, B., "The Evolution of an Elliptic Vortex Ring," *Journal of Fluid Mechanics*, Vol. 109, 1981, pp. 189–216.

[10]Koshigoe, S., Gutmark, E., Schadow, K. C., and Tubis, A., "Wave Structures in Jets of Arbitrary Shape. Part III. Triangular Jets," *Physics of Fluids*, Vol. 31, No. 6, June 1988, pp. 1410–1419.

[11]Cohen, J., and Wygnanski, I., "The Evolution of Instabilities in the Axisymmetric Jet," *Journal of Fluid Mechanics*, Vol. 176, 1987, p. 191.

[12]Gutmark, E., Schadow, K. C., Parr, D. M., and Wilson, K. J., "Noncircular Jets in Combustion Systems," *Experiments in Fluids*, Vol. 7, 1989, pp. 248–258.

[13]Sivasegaram, S., Whitelaw, J. H., Schadow, K. C., and Gutmark, E., "Oscillations in Non-Axisymmetric Dump Combustor," AGARD-CP-450, April 1989, pp. 15-1–15-12.

[14]Schadow, K. C., Gutmark, E., Parr, T. P., Parr, D. M., and Wilson, K. J., "Large-Scale Coherent Structures as Drivers of Combustion Instability," *Combustion Science and Technology*, Vol. 64, No. 4–6, 1989, pp. 167–186.

[15]Kailasanath, K., Gardner, J., Boris, J., and Oran, E., "Interactions Between Acoustics and Vortex Structures in a Central Dump Combuster," *Journal of Propulsion and Power*, Vol. 2, No. 6, 1987, pp. 525–533.

[16]Glass, D. R., "Effects of Acoustics Feedback in the Spread and Decay of Supersonic, Jets," *AIAA Journal*, Vol. 6, No. 10, 1986, pp. 1890–1897.